Surface-structure dependence of water-related adsorbates on platinum

Badan, C.

Chapter 5

Surface Structure Dependence in Desorption and Crystallization of Thin Interfacial Water Films on Pt

5.1 Abstract

In this work we study the influence of substrate structure on desorption and crystallization of water deposited at 100 K on Pt. We use ultrathin water films adsorbed to well-defined, but highly corrugated Pt(211) and Pt(221) surfaces. Desorption spectra reveal variations in the wetting and subsequent layers that critically depend on step type. Crystallization is induced at much lower substrate temperatures as compared to Pt(111). The CI-like layer is also significantly more stable on stepped surfaces as evidenced by a higher desorption energy. Crystallinity of the CI-like layers is maintained over a thickness that varies strongly with step type.

Based on: Badan, C.; Heyrich, Y.; Koper, M. T. M.; Juurlink, L. B. F., J. Phys. Chem. Lett., 2016, 1682-1685

5.2 Introduction

Adsorption of water onto surfaces has been studied in great detail and reviewed several times over the past decades[1–3]. On cold (< 120 K) surfaces, it forms metastable amorphous solid water (ASW)[4–7]. ASW is considered relevant to chemical, biological, physical, astrophysical and material sciences [8–14]. ASW undergoes a phase transformation into crystalline ice (CI) upon heating. This transformation can be detected by temperature programmed desorption (TPD) as a TPD spectrum shows a deflection[4, 15] when the desorption rate drops due to the lower vapor pressure of CI[16].

Water in contact with platinum is often studied in relation to electrochemistry. Pt has good catalytic properties for many electrochemical reactions[17]. It has also become a general model system for the water-metal interface as the interaction amongst water molecules is delicately balanced by the interaction with the substrate [1]. For studies of ASW, CI and the kinetics of the phase transition, the atomically flat Pt(111) plane has often been used[6, 15, 18]. The role of surface corrugation has received more attention only recently. Water molecules tend to gather at steps on Pt(111) surfaces[19]. Steps also enhance ASW crystallization [20], control the formation of ice I_h and I_c[13], and influence long-range interaction in water films[21].

In this paper, we present results comparing ultrathin water layer desorption and crystallization from two stepped platinum surfaces with extremely narrow (111) terraces. These terraces are too narrow to support the preferred hexagonal base unit of CI without interference of the steps. Using such Pt samples, we not only incorporate edges between planes at densities similar to those on actual nanoparticles, we also test whether one may tune properties of interfacial ice through substrate structure. We compare results of TPD measurements for surfaces with different step types but similar step densities and use Pt(111) as our reference.

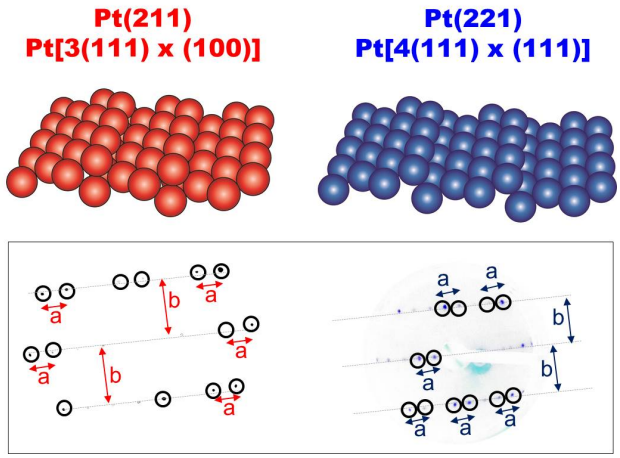

Figure 5.1: Schematic representations and inverted LEED patterns of clean Pt(211) (red) and Pt(221) (blue) on the left and right panels, respectively.

5.3 Experimental Section

Experiments were performed using a home-built (UHV) system with a base pressure of 5×10^{-11} mbar. The system and our standard procedures are discussed in detail elsewhere [22]. Briefly, a quadrupole mass spectrometer (QMS, Baltzers QMA 400) is placed in a differentially pumped canister that connects to the main UHV chamber via a 5 mm diameter circular orifice. The apparatus also contains LEED optics (VG RVL 900), a sputter gun (Prevac IS40C-PS) and three directional dosers. During water (Milipore, 18.2 Ω) deposition, the sample is positioned in front of the capillary array doser with an aperture area that ensures a homogeneous flow over the cleaned sample. Our samples are Pt single crystals (Surface Preparation Laboratory, Zaandam, the Netherlands) of 10 mm diameter and 1 mm thick, with a purity better than 5N and an orientation alignment better than 0.1°). They are positioned 2 mm from the QMS canister's orifice for TPD measurements. Samples are heated radiatively by a filament (Osram, 250 W) positioned behind the crystal or by electron bombardment. Samples are cooled by their connection to a liquid nitrogen reservoir. For all samples, experiments are performed in the same UHV chamber with the same thermocouple connections and the same measurement conditions. We have performed LEED studies on all surfaces. The bare surfaces show the expected diffraction patterns. For the stepped surfaces, we find no evidence for long-range order in the adsorbate

after water adsorption, in line with poor ordering recently observed for H_2O on Pt(553)[23].

5.4 Results and discussion

The top panel of figure 5.1 shows schematic representations of Pt(211)[22] and Pt(221). They are described as consisting of 3 atom wide (111) terraces with (100) steps, and 4 atom wide (111) terraces with (111) steps. The latter description is identical to a 3 atom wide terrace with a (110) step. The bottom panel shows color-inverted photographs of LEED patterns observed for the clean surfaces. From these images we extract spot row spacing (b) to spot splitting (a) ratios of 2.38 for Pt(211) and 3.06 for Pt(221). These values correspond well to literature values of 2.45 and 3.00 [24]. It indicates long-range order with the expected average terrace width for both surfaces.

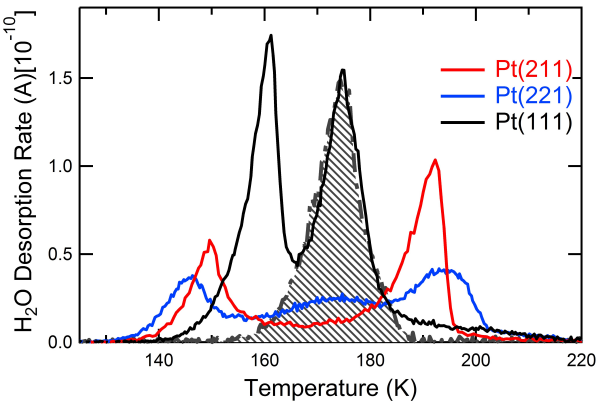

Figure 5.2: TPD spectra of water desorbing from Pt(111), Pt(211) and Pt(221). For TPD experiments the heating rate is 0.91 K s^{-1} over the temperature range shown here.

Figure 5.2 shows TPD spectra of 1 - 2 ML water desorbing from Pt(111), Pt(211), and Pt(221). Desorption between $\sim$ 140 and 165 K results from water adsorbed onto the wetting layer, which is in direct contact with the metal. This 'multilayer' desorption will be discussed below in detail. The crossed area in figure 5.2 corresponds to our best estimate for the complete H_2O wetting layer on Pt(111) and serves as our reference. We refer to it is as 1 $ML^{(111)}$. The small tail in its TPD spectrum at $>$ 190 K is a signature of surface imperfections, such as steps and kinks[25, 26], but may also result in part from a long vacuum time

constant for H_2O. We ignore it in our calibration. Based on various fittings and integrations of the peaks in the Pt(111) spectrum, we estimate our reference to be accurately determined to within $\sim 7\%$. This reference is subsequently used to determine relative coverages in desorption experiments from the other Pt surfaces.

Similar to stepped Pt surfaces with broader terraces [25, 27], Pt(211) and Pt(221) exhibit a clear desorption feature at ~ 194 K. It is attributed to desorption of water molecules adsorbed at step sites [25, 28]. However, the size of this peak varies significantly. As compared to Pt(211), the smaller size of this peak for Pt(221) is balanced by a distinct desorption feature at ~ 174 K, which is characteristic of water desorbing from Pt(111) terraces. This latter peak is also observed on Pt(553)[23, 27], which has the same (111) step type, but a 1-atom wider terrace. The separate appearance of two desorption peaks for these surfaces suggests that water bound to the (111) step and water adsorbed on the (111) terrace are poorly coupled. It may reflect the stable, square arrangement of water molecules in two parallel strands decorating the upper and lower edge of the (111) step[23]. This structure does not provide a good anchor for stable hexagonally-arranged structures on the Pt(111) terrace.

In contrary to Pt(221), Pt(211) does not give rise to a clear desorption peak around 174 K. However, a series of (100)-stepped Pt surfaces up to 8-atom wide terraces[21] do exhibit a distinct peak here, although it is poorly developed for Pt(533)[22]. The absence on Pt(211) thus seems related to the extreme narrow terrace width of Pt(211). Endo et al. and Nakamura et al. have proposed that H_2O_{ad} initially forms a 1-dimensional zig-zag line along the top edge of (100) step sites for Pt(211)[29, 30]. For higher coverages and a 1-atom wider terrace, density functional theory (DFT) calculations show multiple stable structures with nearly identical energies, all containing linear double-stranded water decorating the (100) step edge[31]. Our TPD spectra thus suggest that, contrary to Pt(221), the Pt(211) surface contains no true (111)-terrace-bound water, likely for a lack of space.

The desorption feature appearing at the lowest temperature in figure 5.2 indicates the presence of second or additional water layers [22, 26, 27, 32]. Our direct comparison of the three surfaces using a single UHV apparatus with identical temperature measurement allow us to observe a clear difference in the onset of this "multilayer" desorption feature. The lateral shift signals that the underlying wetting layer and, thus, the metal surface structure tune the desorption of additional water layers. To determine how far the influence of the surface structure reaches into an adsorbed water multilayer, we investigated the desorption of ultrathin layers up to 10 ML^{111} average thickness.

Figure 5.3 displays TPD spectra for Pt(211) and Pt(221) in the top and bot-

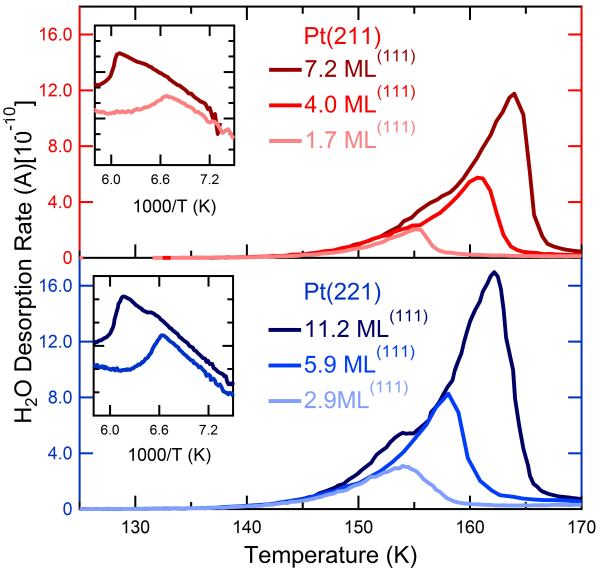

Figure 5.3: TPD spectra of water desorbing from clean Pt(211) (red) and Pt(221) (blue), on the top and bottom panels, respectively. Note that only multilayer desorption features are shown. The inset figures exhibit the Arrhenius plots from the TPD data.

tom panels, respectively. For clarity, we only present the multilayer desorption regime (< 170 K). A typical multilayer desorption spectrum exhibits an exponential increase in desorption rate as a function of temperature with zero-order desorption kinetics [4, 6, 22, 27]. The leading edges for Pt(211) and Pt(221) in figure 5.3 also display a deflection at $\sim$ 156 K and 152 K, respectively, for the largest coverages shown here. After the deflection, the desorption rates align with the traces for lower coverages. This deflection has been well-studied for thick layers of water grown on Pt(111) and other surfaces and indicates crystallization of ASW to CI. [4–6, 25, 32, 33].

The insets in figure 5.3 show typical Arrhenius plots obtained from the same set of TPD spectra. Applying the Arrhenius rate equation, desorption rate = $\nu_0 \times \exp(-E_{des}/RT)$, we extract activation energies (E_{des}) from the slopes of the traces. These activation energies are interpreted as desorption energies. We do this separately for the temperature regimes where the TPD spectra suggest that we observe desorption from two distinct water phases, i.e. prior to and beyond the inflection[5]. We repeat this for various water films grown in the 1-10 ML$^{(111)}$ range. The same analysis also yields frequency factors.

The obtained desorption energies are displayed in figure 5.4 as a function of the (average) water layer thicknesses expressed in terms of our 1 $ML^{(111)}$ reference. The solid lines passing through our data only guide the eye, although the horizontal parts are based on local averages of the data. The horizontal dotted lines are the reported values for E_{des} of ASW and CI grown on Pt(111) [5, 6]. The drop in desorption energy over a narrow range of layer thickness and the rather similar values in comparison the CI and ASW at low and high coverage respectively, strongly suggests that we indeed have two different phases of water desorbing from our samples. As we do not have other means to determine the structure, we refer to them as ASW and crystalline ice-like (CI-like) water.

Comparing the values for E_{des} found for the thicker layers, we find that both stepped surfaces yield values ca. 1 kJ mol^{-1} lower than reported values for ASW. The minor difference is likely a result of the very limited temperature regime over which we need to fit our data as a consequence of using ultrathin films. At the same time, for the thinnest multilayers our values exceed the value reported for CI [5, 6, 34]. We obtain 57.9 and 56.7 kJ mol^{-1} for Pt(211) and Pt(221), respectively, which is to be compared to 55.9 kJ mol^{-1} for Pt(111) [5]. Again, our values may be influenced by limitations resulting from the low film thickness. Nevertheless, the clear difference between the obtained results even for the same layer thickness suggests that our very thin CI-like layers are not quite the same as bulk CI. In addition, the layer thickness required to start observing desorption from an ASW phase differs by a factor of two between the two surfaces. The CI-like phase is ~ 6 monolayers thick on Pt(221) and only ~ 3 ML on Pt(211). Finally, recognizing that variations between different laboratories occur in establishing desorption energies, we note that the absolute difference between CI-like and ASW layers for our stepped surfaces is significantly larger than that for Pt(111). Hence, if the desorption energy of ASW for our stepped surfaces is off and should align with the indicated value for Pt(111), then the CI-like layers on our stepped surfaces are stabilized even more as compared to Pt(111). Obviously, this only holds if the ASW in our ultrathin layers is structurally the same as thick ASW layers.

Crystallization of ASW depends, amongst other variables, on film thickness and desorption rate[7]. For thicker films and low evaporation rates, it occurs at the interface with the vacuum [7, 32, 35]. For ultrathin films, such as those used in this study, it may be expected to occur at the interface with the substrate [7, 15]. If in our experiment ASW is formed upon deposition of water at 100 K, then the surface structure here clearly influences the crystallization rate. On Pt(221) the rate is considerably higher than on Pt(211). On the former, a thicker initial ASW layer is required for ASW to survive while progressing through the temperature

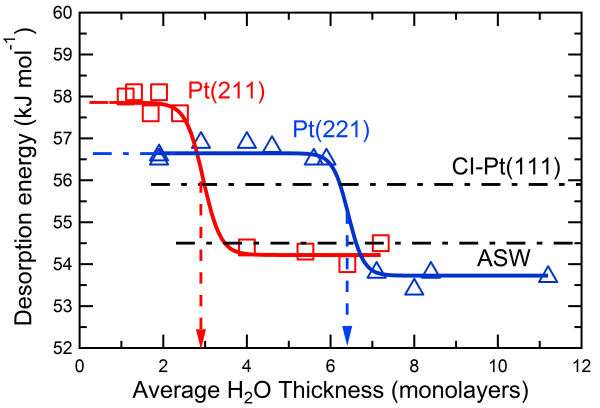

Figure 5.4: Energies for desorption at different water coverages on clean Pt(211) (red squares) and Pt(221) (blue triangles) [22]. The dash-dotted lines are the literature values for the average desorption energies for CI and ASW on Pt(111)[5, 6, 34]. The solid lines fitted through the data are only a guide for the eye.

ramp and exhibiting its specific desorption characteristics in TPD spectra. Higher crystallization rates may reflect more inhomogeneity in the film[4, 15].

On the other hand, the high level of corrugation of the Pt surfaces is not expected to provide sites large enough for CI nuclei to form. The critical radius for nucleation is estimated to be 0.6 +/- 0.4 nm [7]. Backus et al. used a Pt(533) surface to shut down potential crystallization at the interface when studying crystallization of thicker layers[32]. That surface has wider terraces than the surface used here. If crystallization is not induced by the temperature ramp, the CI-like desorption for the first layers on both surfaces indicates that water forms a crystalline structure upon deposition at 100 K. Crystallinity is maintained over various layer thicknesses depending on the details of the structure of the wetting layer and ASW grows on top of the thin CI-like layer. This stacked two-phase model may appear at odds with previous observations of crystalline growth of water deposited at 100 K on CI [15], but the CI-like layers on our nano-structured surfaces are likely not of an ice I type as both clearly show higher desorption energies.

5.5 Conclusions

Concluding, we find significant differences in thermal desorption characteristics for ultrathin water films grown on two similarly stepped Pt(111) surfaces. Differences in comparison to the extended (111) plane are even larger. The step type clearly

affects the structure of interfacial water both in the monolayer and thin film regime. We find CI-like phases at the interface which have a significantly higher desorption energy than bulk CI. We suggest that crystalline adsorption induced by the high level of corrugation at 100 K explains why crystallinity is maintained over different distances into the bulk and depends on details of the type of corrugation. However, we can not exclude that crystallization occurs at the interface during the temperature ramp. In that case, the differences in desorption rate still reflect variations in ASW structure in the layers nearest the surface.

5.6 Bibliography

References

(1) Hodgson, A.; Haq, S. *Surface Science Reports* **2009**, *64*, 381–451.

(2) Henderson, M. A. *Surface Science Rep.* **2002**, *46*, 1–308.

(3) Thiel, P. A.; Madey, T. E. *Surface Science Reports* **1987**, *7*, 211–385.

(4) Smith, R. S.; Huang, C; Wong, E. K. L.; Kay, B. D. *Surface Science* **1996**, *367*, L13–L18.

(5) Smith, R. S.; Matthiesen, J.; Knox, J.; Kay, B. D. *Journal of Physical Chemistry A* **2011**, *115*, 5908–5917.

(6) Löfgren, P.; Ahlström, P.; Lausma, J.; Kasemo, B.; Chakarov, D. *Langmuir* **2003**, *19*, 265–274.

(7) Ahlstrom, P.; Lofgren, P.; Lausma, J.; Kasemo, B.; Chakarov, D. *Physical Chemistry Chemical Physics* **2004**, *6*, 1890–1898.

(8) Ghormley, J. A.; Hochanadel, C. J. *Science* **1971**, *171*, 62–64.

(9) Fecht, H. J. *Nature* **1992**, *356*, 133–135.

(10) Stevenson, K. P.; Kimmel, G. A.; Dohnalek, Z; Smith, R. S.; Kay, B. D. *Science* **1999**, *283*, 1505–1507.

(11) Auslaender, O. M.; Yacoby, A; de Picciotto, R; Baldwin, K. W.; Pfeiffer, L. N.; West, K. W. *Science* **2002**, *295*, 825–828.

(12) Levinger, N. E. *Science* **2002**, *298*, 1722–1723.

(13) Thürmer, K.; Nie, S. *Proceedings of the National Academy of Sciences of the United States of America* **2013**, *110*, 11757–11762.

(14) Svishchev, I. M.; Kusalik, P. G. *Journal of the American Chemical Society* **1996**, *118*, 649–654.

(15) Löfgren, P; Ahlström, P; Chakarov, D. *Surface Science* **1996**, *367*, L19–L25.

(16) Kouchi, A. *Nature* **1987**, *330*, 550–552.

(17) Koper, M. T. M. *Nanoscale* **2011**, *3*, 2054–2073.

(18) Haq, S.; Harnett, J.; Hodgson, A. *Surface Science* **2002**, *505*, 171–182.

(19) Morgenstern, M; Michely, T; Comsa, G *Physical Review Letters* **1996**, *77*, 703–706.

(20) Picolin, A.; Busse, C.; Redinger, A.; Morgenstern, M.; Michely, T. *The Journal of Physical Chemistry C* **2009**, *113*, 691–697.

(21) Den Dunnen, A.; van der Niet, M. J. T. C.; Badan, C.; Koper, M. T. M.; Juurlink, L. B. F. *Physical Chemistry Chemical Physics* **2014**, 8530–8537.

(22) Badan, C.; Koper, M. T. M.; Juurlink, L. B. F. *The Journal of Physical Chemistry C* **2015**, *119*, 13551–13560.

(23) Kolb, M. J.; Farber, R. G.; Derouin, J.; Badan, C.; Calle-Vallejo, F.; Juurlink, L. B. F.; Killelea, D. R.; Koper, M. T. M. *Physical Review Letters* **2016**, *116*, 136101.

(24) Vanhove, M. A.; Somorjai, G. A. *Surface Science* **1980**, *92*, 489–518.

(25) Grecea, M. L.; Backus, E. H. G.; Riedmuller, B; Eichler, A; Kleyn, A. W.; Bonn, M *Journal of Physical Chemistry B* **2004**, *108*, 12575–12582.

(26) Gee, A. T.; Hayden, B. E.; Mormiche, C; Nunney, T. S. English *Journal of Chemical Physics* **2000**, *112*, 7660–7668.

(27) Van der Niet, M. J. T. C.; den Dunnen, A.; Juurlink, L. B. F.; Koper, M. T. M. *Journal of Chemical Physics* **2010**, *132*, 174705–174713.

(28) Skelton, D. C.; Tobin, R. G.; Fisher, G. B.; Lambert, D. K.; DiMaggio, C. L. *Journal of Physical Chemistry B* **2000**, *104*, 548–553.

(29) Endo, O.; Nakamura, M.; Sumii, R.; Amemiya, K. *Journal of Physical Chemistry C* **2012**, *116*, 13980–13984.

(30) Nakamura, M.; Sato, N.; Hoshi, N.; Soon, J. M.; Sakata, O. *Journal of Physical Chemistry C* **2009**, *113*, 4538–4542.

(31) Kolb, M. J.; Wermink, J.; Calle-Vallejo, F.; Juurlink, L. B. F.; Koper, M. T. M. *Physical Chemistry Chemical Physics* **2015**, DOI: 10.1039/C5CP04468E.

(32) Backus, E. H. G.; Grecea, M. L.; Kleyn, A. W.; Bonn, M. *Physical Review Letters* **2004**, *92*, 236101–236104.

(33) Kimmel, G. A.; Petrik, N. G.; Dohnalek, Z.; Kay, B. D. *Journal of Chemical Physics* **2007**, *126*, 114702–114712.

(34) Kimmel, G. A.; Ciolli, R. L.; Stevenson, K. P.; Smith, R. S.; Dohnálek, Z. *Journal of Chemical Physics* **2000**, *112*, 5932–5941.

(35) Wu, Y. C.; Kallis, A.; Jiang, J.; Coleman, P. G. *Physical Review Letters* **2010**, *105*, 066103–066106.